

Laser intensity noise suppression for space-borne gravitational wave mission

FAN LI,¹ XIN SHANG,¹ ZHENGLI MA,¹ JIAWEI WANG,¹ LONG TIAN,^{1,3,5} SHAOPING SHI,¹ WANGBAO YIN,^{2,3} YUHANG LI,⁴ YAJUN WANG,^{1,3} AND YAOHUI ZHENG^{1,3,6}

¹State Key Laboratory of Quantum Optics and Quantum Optics Devices, Institute of Opto-Electronics, Shanxi University, Taiyuan, 030006, China

²State Key Laboratory of Quantum Optics and Quantum Optics Devices, Institute of Laser Spectroscopy, Shanxi University, Taiyuan, Shanxi 030006, China

³Collaborative Innovation Center of Extreme Optics, Shanxi University, Taiyuan 030006, China

⁴State Key Laboratory of Precision Measurement Technology and Instruments, Department of Precision Instrument, Tsinghua University, Beijing 100084, China

⁵tianlong@sxu.edu.cn

⁶yhzheng@sxu.edu.cn

Abstract: Laser intensity noise is a main limitation of measurement and sensing mission represented by gravitational wave detection. We develop a noise decomposition model and design the core elements of the feedback loop independently based on the analysis results. We construct a fiber amplifier system with ultra-low intensity noise in the 0.1 mHz-1 Hz frequency band by the employment of an optoelectronic feedback loop that is specially designed, the relative intensity noise is less than $6 \times 10^{-5} / \sqrt{\text{Hz}}$ @0.1 mHz-1 Hz. By precise control of the temperature and stress, we improve the temperature and mechanical stability of fiber amplifier chain, the differential phase noise reaches $5 \times 10^{-2} \text{ rad} / \sqrt{\text{Hz}}$ @0.1 mHz-1 Hz. The study provides experimental basis and technologies for precise measurement and sensing system at ultra-low frequency.

1. Introduction

The first direct observation of a gravitational wave in 2015 ushered a new era of the universe [1]. Further studies focus on a new generation of ground-based gravitational wave observatory (GWO) with significantly increased sensitivity [2, 3], and space-borne GWO with extended frequency range [4–6], expecting to unlock the detection of more distant and fainter astronomical events. As a critical element of laser interferometer, laser intensity noise and output power are the main limitations of the ground-based and space-borne GWOs. The requirement of gravitational wave (GW) detection continues to drive the laser performance boost. In addition, the development of low-noise, single-frequency laser will also propel the performance of coherent communication and remote detection forward [7–9].

Depending on the specific measurement and sensing mission, there are detailed requirements for laser specifications. Driven by ground-based GWO, the performance of single-frequency laser continues to improve, covering the output power, intensity noise and linewidth and so on [10]. By employment of the master oscillator power amplifier (MOPA) configuration, the output power of the fiber amplifier has reached 1010 W at 1030 nm based on mode field manipulation technology [11]. Another independent topic is intensity noise suppression by a choice of seed laser and low-noise feedback control [12]. NASA Goddard Space Flight Center (GSFC) compared the influence of different kinds of master oscillator lasers, including fiber distributed Bragg reflector laser, Non-Planar Ring Oscillator (NPRO) laser, external cavity diode laser, and fiber ring cavity laser on laser intensity noise [13]. Following the comparison, the same group drew a conclusion that the micro-NPRO laser was an excellent candidate of seed laser for the application of GWO [14]. In addition, integrating with feedback control technology, the intensity noise of fiber amplifier was effectively suppressed at the low-frequency band [15–17]. In consideration of

the influence of signal to noise ratio of feedback loop on ultimate intensity noise, innovative error signal extraction schemes, including high-power photodiode array [18], Optical AC coupling [19], and squeezing-assisted detection [20], have been demonstrated. Currently, the relative intensity noise (RIN) approximately approaches to $2 \times 10^{-9}/\sqrt{\text{Hz}}$ at Fourier frequency of 1 Hz to 10 kHz.

For the mission of space-borne GWO [21], the laser intensity noise suppression at the lower frequency band (0.1 mHz-1 Hz) is urgent to address. Moreover, the differential phase noise of fiber amplifier at 2.4 GHz should be evaluated to satisfy the clock synchronization requirement of the inter-satellite link. In fact, starting from the laser interferometer space antenna (LISA) mission [4], relevant works about laser development are still on the way to higher performance. Until mid-2022, a laser system with MOPA architecture was reported by GSFC, including two low-noise micro-NPRO seed lasers and a one-stage fiber amplifier [22]. The RIN of laser system was approximately $2 \times 10^{-4}/\sqrt{\text{Hz}}$ @0.1 mHz-1 Hz. Subsequently, the RIN of laser system was further suppressed to $1.5 \times 10^{-4}/\sqrt{\text{Hz}}$ at a lower frequency 0.1 mHz [23], which was very close but below the mark of LISA mission $1 \times 10^{-4}/\sqrt{\text{Hz}}$ @0.1 mHz-1 Hz. Notably, the further improvement of the RIN faces a great challenge, especially at the ultra-low frequency 0.1 mHz.

In this paper, we demonstrate a fiber amplifier system with the RIN of $6 \times 10^{-5}/\sqrt{\text{Hz}}$ @0.1 mHz-1 Hz by the employment of an optoelectronic feedback loop, which meets the requirement for space-borne GWOs. According to feedback control theory, we construct a noise decomposition model, quantitatively obtaining the specification requirement for core elements (voltage reference, photodetector etc.) in the loop. Further, we design independently these core elements, integrate these electric units with fiber amplifier, and construct an ultra-low intensity noise fiber amplifier system. Exploiting a passive-stabilized scheme, the differential phase noise is suppressed to $5 \times 10^{-2} \text{ rad}/\sqrt{\text{Hz}}$ @0.1 mHz-1 Hz, which is close to the requirement for space-borne GWOs. These design schemes, results, technical intricacies and the low-noise single frequency fiber amplifier system provide experimental basis and technologies for precise measurement system at ultra-low frequency.

2. Power stabilization noise model

MOPA structure is selected for our low-noise fiber laser amplifier system, which adopts large mode field area double cladding ytterbium doped gain fiber as well as cladding pumping technology. Following the previous studies [24–26], the RIN of laser amplifier at a low frequency band mainly comes from its pump noise, not the noise of seed laser. Therefore, we employ the pump driver of laser amplifier as the actuator of the feedback loop.

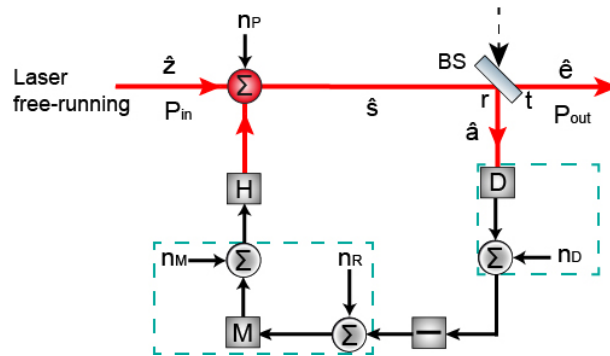


Fig. 1. Schematic representation of power stabilization noise model.

The noise suppression scheme is based on the active feedback loop, as shown in Fig 1. \hat{z} is the input laser field and the input power is denoted by P_{in} . The technical noise introduced by the

fiber amplifier is included in \hat{z} . The pump noise introduced by the actuator in the active control loop is denoted by n_P . The field \hat{s} after the actuator extracts a small fraction of the light into the photodetector through a beam splitter (BS). The signal measured by the photodetector is applied to the actuator through feedback to cancel the power fluctuation signal. Also consider a lossless BS, i.e. $r^2 + t^2 = 1$. \hat{a} (r^2 and t^2 represent the power reflectivity and power transmissivity, respectively.). \hat{a} is the in-loop laser field, \hat{e} is the out of loop laser field and the output power is denoted by P_{out} . In addition, the feedback loop gain is represented by the detector gain D , the controller gain M , and the actuator gain H , respectively, i.e., $G = HMD$. n_D , n_D and n_R represent the fluctuations from the detector and reference in the feedback loop, respectively. n_M is the fluctuation introduced by the controller. The amplitude quadrature of the output noise field is expressed in Eqs (1)-(2):

$$\hat{s} = \hat{z} + n_P + Hn_M + HMn_R - HMn_D - HMD\hat{a} \quad (1)$$

$$\hat{e} = \frac{t(\hat{z} + n_P)}{1 + rG} + \frac{tH}{1 + rG}n_M + \frac{tG}{1 + rG}\frac{n_R}{D} - \frac{tG}{1 + rG}\frac{n_D}{D} \quad (2)$$

Assuming that all inputs to the system are uncorrelated, the power spectral density quadrature to the amplitude of the output field can be calculated in Eq (3). where $\gamma_{n_R}^2$, $\gamma_{n_M}^2$, and $\gamma_{n_D}^2$ represent the electronic noise contribution in V^2/Hz , respectively. PSD_{tech} is the sum of actuator noise and input field noise, and so:

$$PSD_{\hat{e}} = \frac{t^2 PSD_{\text{tech}}}{|1 + rG|^2} + \frac{t^2 |H|^2 \gamma_{n_M}^2}{|1 + rG|^2} + \frac{t^2 |G|^2}{|1 + rG|^2} \frac{\gamma_{n_R}^2}{|D|^2} + \frac{t^2 |G|^2}{|1 + rG|^2} \frac{\gamma_{n_D}^2}{|D|^2} \quad (3)$$

Next, defining the RIN of the output field \hat{e} [27], where the output field's carrier power is given by $P_{\text{out}} = t^2 P_{\text{in}}$. The RIN of the output field is expressed in Eqs (4)-(5) :

$$RIN_{\hat{e}}^2 = \frac{2h\omega}{P_{\text{out}}} PSD_{\hat{e}} = \frac{2h\omega}{t^2 P_{\text{in}}} PSD_{\hat{e}} \quad (4)$$

$$RIN_{\hat{e}}^2 = \frac{RIN_{\text{tech}}^2}{|1 + rG|^2} + \frac{2h\omega}{P_{\text{in}}} \frac{|H|^2 \gamma_{n_M}^2}{|1 + rG|^2} + \frac{2h\omega}{P_{\text{in}}} \frac{|G|^2}{|1 + rG|^2} \frac{\gamma_{n_R}^2}{|D|^2} + \frac{2h\omega}{P_{\text{in}}} \frac{|G|^2}{|1 + rG|^2} \frac{\gamma_{n_D}^2}{|D|^2} \quad (5)$$

Where h is the Planck constant, ω is the optical angular frequency. From Eq (5), the RIN comes from the contribution of residual technology noise, controller noise, voltage reference noise and photodetector electronics noise, respectively. For large loop gains ($G \gg 1$), the influence of the residual technical noise RPN_{tech}^2 and the controller noise $\gamma_{n_M}^2$ on the RIN can be neglected, the voltage reference noise $\gamma_{n_R}^2$ and photodetector electronics noise $\gamma_{n_D}^2$ is main limitation of the RIN. The conclusion points out our direction of the experimental realization.

3. Experimental setup

Fig. 2 shows the experimental setup of our laser amplifier system. The laser amplifier consists of laser amplifier unit (LAU), active stabilization unit (ASU), and electrical acquisition and control unit (EACU). The LAU and ASU are independently placed on an insulation house with active temperature control.

A NPRO with a center wavelength of 1064 nm and an output power of 500 mW serves as its seed source (not shown in the Fig. 2), and after free space attenuation, 50 mW of optical power is injected into the laser amplifier. Two series-connected 976 nm laser diodes (Aerodiode, 976 LD, 10 W-105 μm) are employed as the pump source for the laser amplifier, which is injected into the gain fiber with the same direction as the seed source after passing through

a $(2 + 1) \times 1$ polarization-maintaining combiner. The gain fiber in the amplifier is a 2.5 m ytterbium-doped double-clad fiber (Nufern, PLMA-YDF-10/125) with 10 μm core diameter, 125 μm pump cladding diameter, and numerical apertures of 0.075 and 0.46 for core and pump cladding, respectively. We use one-component silicon to secure the gain fiber to a copper heat sink with U-shaped grooves etched into it, and precisely control the temperature of the copper heat sink. To reduce the influence of the residual 976 nm pump light on the downstream main laser, we used a cladding pump stripper (CPS) at the end link of the gain fiber. Furthermore, a polarization-maintaining fiber optic isolator (ISO) is installed in the output of the seed laser and the output of the amplifier respectively, which significantly reduces the influence of backscattered light on the output signal light. The other side of the ISO is the elimination of parasitic interference, improving the low-frequency performance of the laser amplifier. These elements mentioned above are installed inside the LAU.

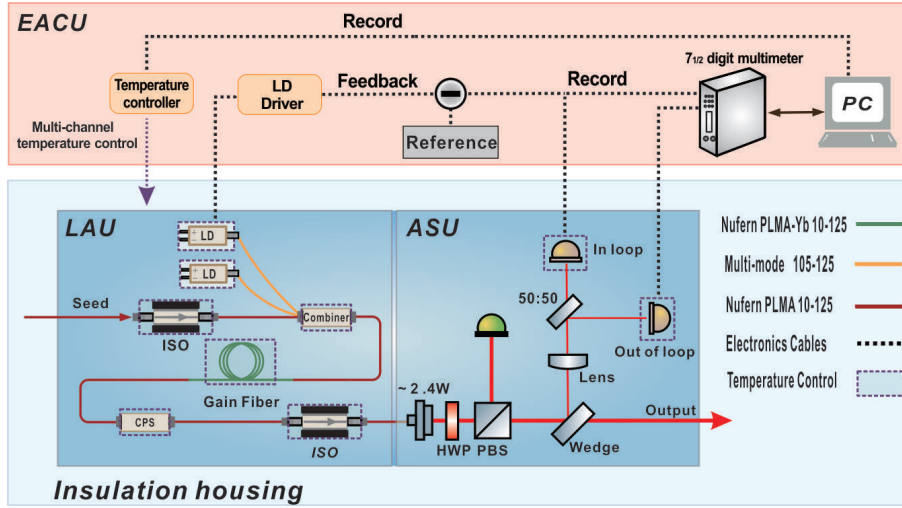


Fig. 2. Experimental setup of low-noise single-frequency laser amplifier system. ISO: Isolator; LAU: laser amplifier unit; ASU: active stabilization unit; EACU: electrical acquisition and control unit.

The output of our fiber amplifier is collimated by a fiber collimator to produce a 2 mm beam in diameter. The laser first passes through a half-wave plate with a polarizing beam splitter (PBS) to obtain a horizontally polarized laser. A wedge splitter is placed after the PBS, and an integrating sphere power meter is used to detect the laser at the transmission end. The laser at the reflection end is focused by a lens with a focal length of 100 mm and then split into two beams by a non-polarizing 50:50 beam splitter. Two home-made low-noise photodetectors are employed as the in-loop and out-of-loop signal acquisition, respectively. The substrate of the 50:50 beam splitter is fused silica, which has a lower coefficient of thermal expansion. To minimize ghosting, the 50:50 beam splitter has a 30 arcmin wedged back surface. These mentioned free-space devices, including fiber collimator, PBS, beam splitters and low-noise photodetectors, are positioned inside the ASU. The electrical component is shown in the upper part of Fig. 2, named as EACU. The EACU includes the voltage reference, current driver, temperature controller etc., which is detailed in Section 5.

4. Characterization of free-running laser amplifier

In free-running mode, we measure the output power of the laser amplifier as a function of the pump power, as shown in Fig. 3(a). The output power increases linearly with the pump power

with a slope efficiency measured of 56.45%. In consideration of the damage threshold of the ISO, the laser amplifier operates at 2.4 W for extended periods. There is no obvious stimulated Brillouin scattering phenomenon at the operating power, and the polarization extinction ratio is above 28 dB. The laser spectrums of the seed laser and laser amplifier are given in Fig. 3(b). The resolution and scanning range of the optical spectrum analyzer (Yokogawa AQ6370D) are set to 0.02 nm and 150 nm, respectively. As observed, the center wavelength of the seed laser is 1064.45 nm with an optical signal-to-noise ratio (OSNR) of 72 dB and no amplified spontaneous emission (ASE) is generated.

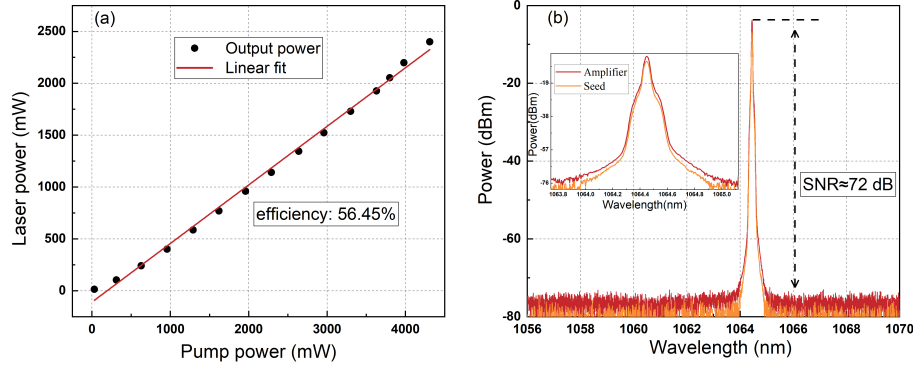


Fig. 3. (a) Output power of the laser amplifier versus pump power. (b) Laser spectra for seed laser and power amplifier.

Here, we mainly focus on the RIN suppression of the laser amplifier. Although the frequency noise is primarily dependent on the seed laser, we also measure the frequency noise of the laser amplifier in order to make a global investigation into the application of space-borne GWOs. Utilizing the optical heterodyne beat-frequency technique [28], we construct the measurement setup and obtain the frequency noise spectrum of the free running laser amplifier, shown in Fig. 4 (a). The result meets the scientific requirement that the LISA mission claims for the frequency noise of the free-running laser [21, 29].

The space-borne GWO needs to transfer clock information among its three spacecraft in the form of 2.4 GHz phase-modulation sidebands [30, 31]. For this reason, the phase noise introduced by the optical chain between the carrier and sideband must be as low as possible [32, 33]. The differential phase noise of laser amplifiers is commonly used as a performance indicator. According to the existing analysis, the differential phase noise originates from the thermal load on the active fiber, thermo-mechanical induced birefringence, nonlinearities in fibers and temperature fluctuations [34]. Especially at ultra-low frequency, the temperature and mechanical fluctuations are the main limitation of the differential phase noise. Here, we construct a high-stability, stress-free stove that has a temperature fluctuation of less than 5 mK, for the fiber amplifier chain to isolate environmental disturbance. Via the passive-stabilized scheme, the differential phase noise is effectively suppressed. The measurement setup for the differential phase noise has been constructed based on reference [35]. Fig. 4(b) shows the measurement result of the differential phase noise. The gray curve is the noise floor of the phasemeter (Moku: lab), which is obtained by recording the phase difference of the same sinusoid signal. By replacing the gain fiber with a short, passive fiber, we record the noise floor of the measurement setup, shown with the blue curve in Fig. 4 (b). The red curve of Fig. 4 (b) is the measurement result of the differential phase noise of the fiber amplifier at the output power of 2.4 W, not subtracting the dark noise. In the future, we expect to suppress the differential phase noise by optimizing the doping concentration and size of gain fiber, and the stove construction [36], to satisfy LISA mission.

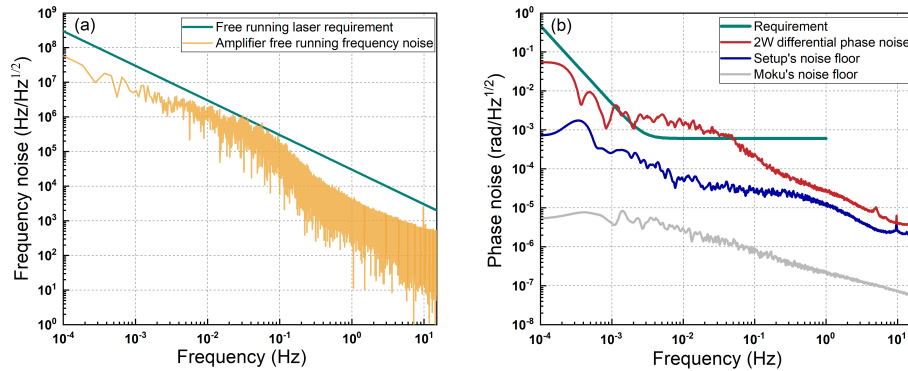


Fig. 4. (a) Frequency noise and (b) differential phase noise of the fiber amplifier in the 0.1 mHz-15 Hz frequency band.

5. Characterization laser amplifier with power stabilization

According to the power stabilization noise model of Section 2, we develop an active feedback control system to suppress the RIN of laser amplifiers in ultra-low frequency bands. We choose the driver of pump laser as an actuator of the feedback loop, which is a general technique [37–39]. As is shown by the EACU in Fig. 2, a photodetector converts a fraction of laser power disturbances into an electrical voltage signal. The signal is subtracted from the reference voltage to obtain the feedback loop error signal, which is amplified and filtered by the servo controller to manipulate the power supply of the pump laser. For our experiment in the 0.1 mHz-1 Hz frequency band, we should pay more attention to the noise coupling of the components in the feedback system, the $1/f$ noise, and the temperature coefficient of the devices, rather than the feedback bandwidth, which distinguishes the high-frequency range power stabilization experiments to some extent.

Based on the analysis in Section 2, we first upgrade the photodetector. Thermoelectrically cooled 5 mm InGaAs photodiodes from Hamamatsu’s G12180-150A are used, which enables both low-noise and low dark current. And the G12180-150A has an internally integrated Thermoelectric Cooler (TEC) that keeps the temperature and responsivity of sensitive area stable. The photodiode operates in photovoltaic mode, which provides lower dark noise without reverse bias. As is shown by the orange curve in Fig. 5 (a), the measured photodetector with an electronic noise γ_{nD}^2 of $9.5 \times 10^{-7}/\sqrt{\text{Hz}}@0.1 \text{ mHz-1 Hz}$. The noise spectrum is relatively flat throughout the frequency range and no significant $1/f$ noise is observed. This is largely due to the zero-drift operational amplifier (Analog Devices LTC1151) used in the TIA circuit, which has a unique chopping technique that effectively reduces the effects of $1/f$ noise. In addition, these excellent performances also benefits from a low noise power supply and a precision low temperature coefficient metal foil resistor.

The voltage reference is another limitation of the RIN of the laser amplifier. The reference voltage provided by the ultra-precision reference (Linear Technology LTZ1000) has an extremely low temperature coefficient, typically less than 0.05 ppm/ $^{\circ}\text{C}$ (up to 0.01 ppm/ $^{\circ}\text{C}$ when equipped with an external temperature controller), meaning that temperature variations have a minimal effect on the output voltage. The purple curve in Fig. 5 (a) shows the relative voltage noise spectral density γ_{nR}^2 of the voltage reference, which is superior to $1 \times 10^{-6}/\sqrt{\text{Hz}}$ in the range of 0.1 mHz-1 Hz. The indicator is two orders of magnitude better than of the RIN requirement, which meets the design requirement. In ideal condition, the influence of the residual technical noise RPN_{tech}^2 and the controller noise γ_{nM}^2 on the RIN can be neglected. However, the actual feedback loop does not have an infinite gain factor. Therefore, we cannot give ourselves an excuse to avoid upgrading the current driver. Integrating the pump driver with controller and actuator circuits on board, we greatly reduce ambient noise coupling, further reduce the residual technical

noise RPN_{tech}^2 and the controller noise γ_{nM}^2 of the laser amplifier system in free-running mode. It is worth noting that our design for the laser driver focuses on the low-frequency performance. Fig. 5 (b) shows the comparison between the home-made driver and commercial ones. The noise level of the home-made driver in the range of 0.1 mHz-5 mHz is significantly lower than that of other commercial drivers, which is relatively flat throughout the concerned frequency range.

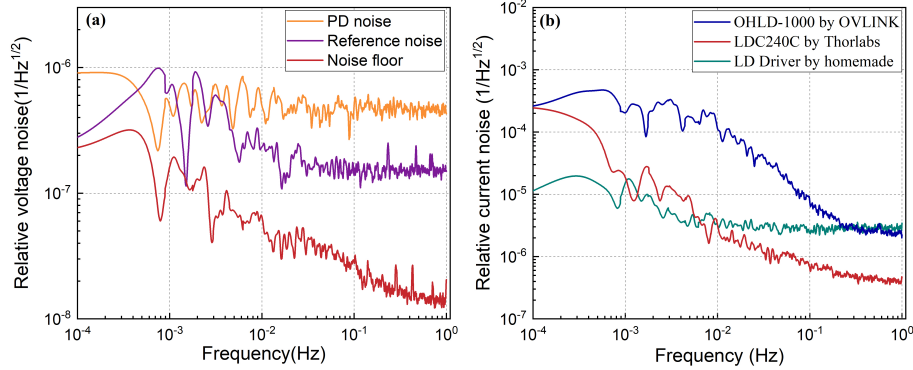


Fig. 5. (a) Voltage reference performance and photodetector dark noise. (b) Comparison of current noise spectral density between homemade and commercial pump drivers.

The red curve of Fig. 6 shows the RIN of the free-running laser amplifier with $4 \times 10^{-3}/\sqrt{\text{Hz}}@0.1 \text{ mHz-1 Hz}$, which is driven by home-made laser driver. In Eq.5, the detector gain D can be expressed as $D = k\sqrt{2h\omega r^2 P_{\text{in}}}$, where k is the photodetector calibration factor ($k=27300\text{V/W}$), which is related to the photodiode responsivity, quantum efficiency and transimpedance resistance. The actual loop gain G varies with frequency in the 0.1 mHz-1 Hz frequency range, but the transfer function of the system at ultra-low frequency cannot be accurately measured with existing instruments. Here, we choose $G = 100$ (assumed to be frequency independent) for calculation, the expected out-of-loop RIN is an uncorrelated superposition of the residual technology noise, the controller noise, the photodetector electronics noise and the reference noise. Instituting these measurement results of each independent element into Eq. 5, we obtain the expected out of loop RIN noise, shown with orange curve in Fig. 6. The blue curve shows the out-of-loop performance of the laser amplifier with RIN of below $6 \times 10^{-5}/\sqrt{\text{Hz}}@0.1 \text{ mHz-1 Hz}$. According to the Eq. 5, the in-loop noise is an uncorrelated superposition of the residual technology noise and the photodetector noise, which is shown by the black curve in Fig.6. It is necessary to note that that out-of-loop noise almost matches the expected value in the 200 mHz-1 Hz range, but at low frequencies ($< 200 \text{ mHz}$) is not as expected. It can be explained that we choose a frequency-independent index G for the calculation, while the actual G is frequency-dependent. Furthermore, in the 10 mHz-1 Hz band, the out-of-loop noise approximately overlaps with the in-loop one. At the lower frequency bands, the out-of-loop noise is inferior to the in-loop one. This phenomenon may be attributed to the residual temperature noise of the Photodiode and the "ghosting" effect resulting from the detector window, photodetector sensitivity fluctuation from beam pointing.

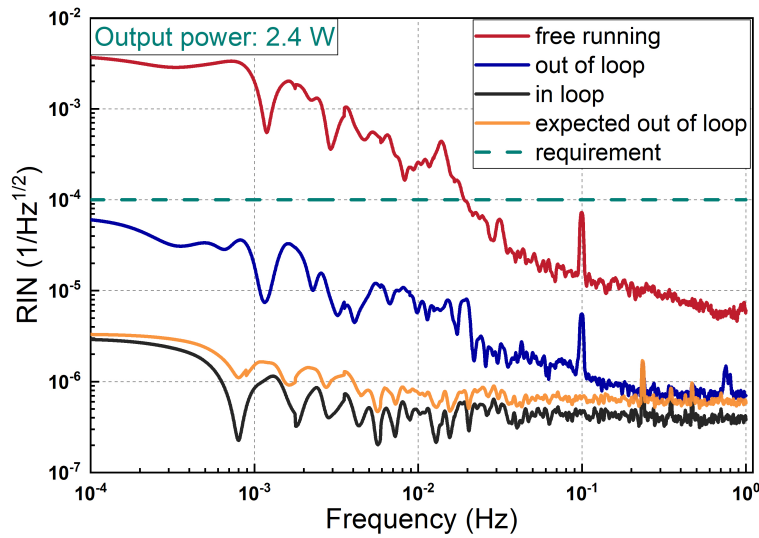


Fig. 6. Relative intensity noise of the laser amplifier.

6. Conclusion

We have demonstrated a fiber amplifier system with 2.4 W output by the employment of an optoelectronic feedback loop and precise temperature control. Starting from feedback control theory, we quantify the specification requirement for core elements. By designing the low-noise voltage reference, photodetector and laser driver in 0.1 mHz-1 Hz frequency band, the RIN of $6 \times 10^{-5}/\sqrt{\text{Hz}}@0.1 \text{ mHz-1 Hz}$ is experimentally obtained, which meet the requirement for space-borne GWOs. By precisely controlling the temperature and stress of the laser amplifier chain, the differential phase noise is suppressed to $5 \times 10^{-2} \text{ rad}/\sqrt{\text{Hz}}@0.1 \text{ mHz-1 Hz}$, which is close to the requirement for space-borne GWOs. The experimental results are in good agreement with analysis ones. The work points out our direction of further performance improvement and offers essential technologies for the noise suppression of laser amplifier at low-frequency band. Relying on advanced techniques for preparing with the help of squeezed and entanglement state [40–43], we expect to further improve the performance of the noise suppression.

Funding. Project supported by the National Key R&D Program of China (Grant No. 2020YFC2200402); National Natural Science Foundation of China (NSFC) (Grants No. 62225504, No. U22A6003, No. 62027821, No. 62035015, No. 12174234, No. 62375162, No. 12304399); Fundamental Research Program of Shanxi Province (No.202303021212003, 202303021224006).

Disclosures. The authors declare no conflicts of interest.

Data Availability Statement. Data underlying the results presented in this paper are not publicly available at this time but may be obtained from the authors upon reasonable request.

References

1. B. P. Abbott, R. Abbott, T. D. Abbott, M. R. Abernathy, F. Acernese, and K. Ackley, et al., “Observation of gravitational waves from a binary black hole merger,” *Phys. Rev. Lett.* **116**(6), 061102 (2016).
2. B. P. Abbott, R. Abbott, T. D. Abbott, M. R. Abernathy, K. Ackley, and C. Adams, et al., “Exploring the Sensitivity of Next Generation Gravitational Wave Detectors,” *Class. Quantum Gravity* **34**(4), 044001 (2017).
3. K. Ackley, V. B. Adya, P. Agrawal, P. Altin, G. Ashton, and M. Bailes, et al., “Neutron star extreme matter observatory: A kilohertz-band gravitational-wave detector in the global network,” *Publ. Astron. Soc. Aust.* **37**, e047 (2020).
4. K. Danzmann, H. Audley, E. Barausse, P. Bender, E. Berti, C. Caprini, N. Cornish, L. Ferraioli, V. Ferroni, E. Fitzsimons, L. G. Boté, F. Gibert, G. Heinzl, T. Hertog, M. Hewitson, N. Korsakova, S. Larson, J. Livas, I. Mateos, S. McWilliams, G. Nardini, A. Petiteau, J. Reiche, G. Russano, J. Slutsky, C. Sopuerta, D. Vetrugno, G. Wanner,

- and J. Ziemer, "LISA Laser Interferometer Space Antenna A proposal in response to the ESA call for L3 mission concepts Lead," (2017).
5. J. Luo, L. Chen, H. Duan, Y. Gong, S. Hu, J. Ji, Q. Liu, J. Mei, V. Milyukov, M. Sazhin, C. Shao, V. T. Toth, H. Tu, Y. Wang, Y. Wang, H. Yeh, M. Zhan, Y. Zhang, V. Zharov, and Z. Zhou, "TianQin: a space-borne gravitational wave detector," *Class. Quantum Gravity* **33**(3), 035010 (2016).
 6. Z. Luo, Y. Wang, Y. Wu, W. Hu, and G. Jin, "The Taiji program: A concise overview," *Prog. Theor. Exp. Phys.* **2021**(5), 05A108 (2021).
 7. O. D. Varona, W. Fittkau, P. Booker, T. Theeg, M. Steinke, D. Kracht, J. Neumann, and P. Wessels, "Single-frequency fiber amplifier at 1.5 μm with 100 W in the linearly-polarized TEM00 mode for next-generation gravitational wave detectors," *Opt. Express* **25**(21), 24880-24892 (2017).
 8. Y. Tao, M. Jiang, L. Liu, C. Li, P. Zhou, and Z. Jiang, "More Than 20 W, High Signal-to-Noise Ratio Single-Frequency All-Polarization-Maintaining Hybrid Brillouin/Ytterbium Fiber Laser," *J. Light. Technology* **41**(2), 678-683 (2023).
 9. F. Wellmann, N. Bode, P. Wessels, L. Overmeyer, J. Neumann, B. Willke, and D. Kracht, "Low noise 400 W coherently combined single frequency laser beam for next generation gravitational wave detectors," *Opt. Express* **29**(7), 10140-10149 (2021).
 10. Jan Hendrik Pödl, "Design, Implementation and Characterization of the Advanced LIGO 200W Laser System," PhD thesis, University of Hannover (2014).
 11. W. Li, P. Ma, Y. Deng, Y. Chen, Q. Chen, W. Liu, H. Xiao, Z. Chen, L. Si, and P. Zhou, "All-fiber single-frequency near-single-mode laser breaks through kilowatt output for the first time," *Chin. J. Lasers* **51**(7), 0716002 (2024).
 12. M. Tröbs, "Laser development and stabilization for the spaceborne interferometric gravitational wave detector LISA," PhD thesis, University of Hannover (2005).
 13. J. B. Camp, K. Numata, and M. A. Krainak, "Progress and Plans for a US Laser System for LISA," *J. Physics: Conf. Ser.* **840**, 012013 (2017).
 14. K. Numata, A. Yu, H. Jiao, S. Merritt, F. Micalizzi, M. Fahey, J. Camp, and M. Krainak, "Laser system development for the LISA (Laser Interferometer Space Antenna) mission," *Proc. SPIE* **10896**, (2019).
 15. J. Zhao, G. Guiraud, C. Pierre, F. Floissat, A. Casanova, A. Hreibi, W. Chaibi, N. Traynor, J. Boulet, and G. Santarelli, "High-power all-fiber ultra-low noise laser," *Appl. Phys. B* **124**(114), (2018).
 16. Z. Wang, J. Wang, F. Li, Y. Li, L. Tian, and Q. Liu, "Yb-Doped All-Fiber Amplifier with Low-Intensity Noise in mHz Range Oriented to Space-Borne Gravitational Wave Detection," *Appl. Sci.* **13**(10), 6338 (2023).
 17. F. Meylahn, N. Knust, and B. Willke, "Stabilized laser system at 1550 nm wavelength for future gravitational-wave detectors," *Phys. Rev. D* **105**, 122004 (2022).
 18. P. Kwee, B. Willke, and K. Danzmann, "Shot-noise-limited laser power stabilization with a high-power photodiode array," *Opt. Lett.* **34**(19), 2912-2914 (2009).
 19. P. Kwee, B. Willke, and K. Danzmann, "Optical ac coupling to overcome limitations in the detection of optical power fluctuations," *Opt. Lett.* **33**(13), 1509-1511 (2008).
 20. H. Vahlbruch, D. Wilken, M. Mechmet, and B. Willke, "Laser Power Stabilization beyond the Shot Noise Limit Using Squeezed Light," *Phys. Rev. Lett.* **121**(17), 173601 (2018).
 21. B. Shortt, L. Mondin, P. McNamara, K. Dahl, S. Lecomte, and P. Duque, "LISA Laser System and European Development Strategy," *Int. Conf. on Space Opt.* (2019).
 22. A. W. Yu, and K. Numata, "Progress of the US Laser Development for the Laser Interferometer Space Antenna (LISA) Program," *IGARSS 2022 - 2022 IEEE Int. Geoscience Remote. Sens. Symposium*, 4276-4279 (2022).
 23. P. Cebeci, M. Giesberts, P. Baer, Jonas Eßer, Joel Guetzlaff, H. Hoffmann, and K. Dahl, "Highly stable fiber amplifier development and environmental component-testing for the space-based gravitational wave detector LISA," *Proc. SPIE* **12400**, 162-167 (2023).
 24. S. Novak, and A. Moesle, "Analytic model for gain modulation in EDFAs," *J. Light. Technology* **20**(6), 975-985 (2002).
 25. H. Tünnermann, J. Neumann, D. Kracht, and P. Weßels, "Gain dynamics and refractive index changes in fiber amplifiers: a frequency domain approach," *Opt. Express* **20**(12), 13539-13550 (2012).
 26. M. Tröbs, P. Weßels, and C. Fallnich, "Power- and frequency-noise characteristics of an Yb-doped fiber amplifier and actuators for stabilization," *Opt. Express* **13**(6), 2224-2235 (2005).
 27. J. R. Venneberg, and B. Willke, "Quantum correlation measurement of laser power noise below shot noise," *Opt. Continuum* **1**, 1077-1084 (2022).
 28. S. Camatel, and V. Ferrero, "Narrow Linewidth CW Laser Phase Noise Characterization Methods for Coherent Transmission System Applications," *J. Light. Technology* **26**(17), 3048-3055 (2008).
 29. L. Karlen, E. Onillon, S. Kundermann, S. Lecomte, K. Numata, M. Rodriguez, A. Yu, B. Shortt, and L. Mondin, "LISA laser head metrology," *Proc. SPIE Int. Soc. Opt. Eng.* **12777**, 127773B (2023).
 30. J. Faller, and P. Bender, "A Possible Laser Gravitational Wave Experiment in Space," *Precis. measurement fundamental constants II*, 689-690 (1984).
 31. M. Tinto, and S. Dhurandhar, "Time-delay interferometry," *Class. Quantum*, S283-S289 (2003).
 32. S. Barke, M. Tröbs, B. Sheard, G. Heinzel, and K. Danzmann, "EOM sideband phase characteristics for the spaceborne gravitational wave detector LISA," *Appl. Phys. B* **98**, 33-39 (2009).
 33. S. Barke, "Inter-spacecraft frequency distribution for future gravitational wave observatories," PhD thesis, University of Hannover (2015).

34. M. Tröbs, S. Barke, T. Theeg, D. Kracht, G. Heinzel, and K. Danzmann, "Differential phase-noise properties of a ytterbium-doped fiber amplifier for the Laser Interferometer Space Antenna," *Opt. Lett.* **35**(3), 435-437 (2010).
35. M. Tröbs, C. Bogan, S. Barke, G. Kuhn, J. Reiche, G. Heinzel, and K. Danzmann, "Transportable setup for amplifier phase fidelity measurements," *J. Physics: Conf. Series.* **610**, 012041 (2015).
36. J. Campbella, X. Xu, D. Poullosb, M. Faheyb, K. Numatab, A. Yu, and P.Dragic, "Investigation into the Origin of the RF Phase Noise for the LISA Laser Transmitter," *Proc.SPIE Int.Soc.Opt.Eng.* **12865** (2024).
37. M. Heurs, V. M. Quetschke, B. Willke, and K. Danzmann, "Simultaneously suppressing frequency and intensity noise in a Nd:YAG nonplanar ring oscillator by means of the current-lock technique," *Opt. Lett.* **29**(18), 2148-2150 (2004).
38. Y. Sun, C. Wang, Q. Zhao, C. Yang, C. Zeng, W. Lin, Z. Feng, Z. Yang, and S. Xu, "10 W super-wideband ultra-low-intensity-noise single-frequency fiber laser at 1 μm ," *Opt. Express* **32**(7), 11419-11428 (2024).
39. J. Rollins, D. Ottaway, M. Zucker, R. Weiss, and R. Abbott, "Solid-state laser intensity stabilization at the 10⁻⁸ level," *Opt. Lett.* **29**(16), 1876-1878 (2004).
40. S. Shi, L. Tian, Y. Wang, Y. Zheng, C. Xie, and K. Peng, "Demonstration of Channel Multiplexing Quantum Communication Exploiting Entangled Sideband Modes," *Phys. Rev. Lett.* **125**(7), 070502 (2020).
41. X. Sun, Y. Wang, Y. Tian, Q. Wang, L. Tian, and Y. Zheng, "Deterministic and Universal Quantum Squeezing Gate with a Teleportation-Like Protocol," *Laser & Photonics Rev.* **16**(3), 2100329 (2021).
42. S. Shi, Y. Wang, L. Tian, W. Li, Y. Wu, Q. Wang, Y. Zheng, and K. Peng, "Continuous Variable Quantum Teleportation Network," *Laser & Photonics Rev.* **17**(2), 2200508 (2022).
43. L. Gao, L. Zheng, B. Lu, S. Shi, L. Tian, and Y. Zheng, "Generation of squeezed vacuum state in the millihertz frequency band," *Light. Sci. & Appl.* **13**, 294 (2024).